Journal of Power Sources 635 (2025) 236527

Contents lists available at ScienceDirect

Journal of Power Sources

journal homepage: www.elsevier.com/locate/jpowsour

In-situ measurement of the thermophysical properties of cylindrical batteries under calibrated iso-flux condition

Ruitong Liu [a], Hengyun Zhang [a,b,*], Jinqi Liu [a], Hong Yu [a], Shen Xu [a], Xinwei Wang [c]

[a] School of Mechanical and Automotive Engineering, Shanghai University of Engineering Science, 333 Longteng Road, Songjiang, Shanghai, 201620, China
[b] Mechanical Industrial Key Laboratory of Boiler Low-Carbon Technology, 333 Longteng Road, Songjiang, Shanghai, 201620, China
[c] Department of Mechanical Engineering, 2025 Black Engineering Building, Iowa State University, Ames, IA, 50011, USA

HIGHLIGHTS

- Theoretical analysis conducted under iso-flux condition for cylindrical battery.
- Thermal protection test method proposed for thermal conductivity and specific heat.
- Radial thermal conductivity and specific heat obtained simultaneously.
- Effective thermal management configurations examined for different battery formats.

ARTICLE INFO

Keywords:
In-situ measurement
Thermal protection setup
Calibrated iso-flux condition
Radial thermal conductivity
Specific heat
Fourier number

ABSTRACT

The thermophysical properties of lithium-ion batteries are significant in the thermal management and thermal safety for electric vehicles (EV). In this paper, an in-situ measurement method of the thermophysical properties focusing on the cylindrical batteries are proposed, in which the thermal protection setup is developed to enable radial thermal conductivity measurements under a calibrated iso-flux condition, with a minimal heat leakage by no more than 3 % during the test period. Based on the theoretical analysis, the radial thermal conductivity of the cylindrical battery is obtained during the transient temperature rise stage, whereas the specific heat is obtained by double exponential fitting during the stage close to the quasi-steady state. The radial thermal conductivity is calculated through matching the one-dimensional thermal simulation results with experimental data. It is indicated that the experimentally obtained specific heat ranges from 987.2 to 1076 J kg^{-1} $°C^{-1}$, increasing proportionally as the radial thermal conductivity rises from 1.147 to 1.250 W m^{-1} $°C^{-1}$ with the temperature ranging from −15 °C to 45 °C. This method possesses the advantages of simultaneous determination of specific heat and normal thermal conductivity with reduced test time and augmented accuracy, which would have profound impact in the analysis and design of battery thermal management.

Nomenclature			
		$T_{\max}$, T_{out}	maximum battery temperature and cold plate temperature (°C)
		v	velocity ($m \cdot s^{-1}$)
A	surface area of the test battery (m^2)	ΔT	average temperature rise of the lateral side of the battery (°C)
A_w	cross-sectional area of the cooling pipeline (m^2)	ΔT_2	average temperature rise of the simulation (°C)
c	specific heat of battery ($J \cdot kg^{-1} \cdot °C^{-1}$)	ΔT_w	water temperature rise (°C)

(*continued on next column*)

(*continued*)

$c_n(t)$	time-dependent coefficients	ΔT_z, ΔT_r	maximum temperature rise for the bottom cooling and lateral cooling (°C)
c_w	specific heat of water ($J \cdot kg^{-1} \cdot °C^{-1}$)	ΔV	the heat flux voltage output by the heat flux sensor (V)
dT/dt	temperature rise rate		
Fo	thermal Fourier number	*Acronyms*	
Fo_1, Fo_2	experimental and numerical Fourier number	ARC	accelerated rate calorimeter

(*continued on next page*)

---

* Corresponding author. School of Mechanical and Automotive Engineering, Shanghai University of Engineering Science, 333 Longteng Road, Songjiang, Shanghai, 201620, China.

E-mail address: zhanghengyun@sues.edu.cn (H. Zhang).

https://doi.org/10.1016/j.jpowsour.2025.236527
Received 26 December 2024; Received in revised form 9 February 2025; Accepted 11 February 2025

(*continued*)

H	height of cylindrical battery (m)	CFD	computational fluid dynamic
J_0,J_1	the zeroth-order and first-order Bessel function of the first kind	C-rate	measurement of the charge and discharge current with respect to its nominal capacity
k	battery's thermal conductivity (W·m^{-1}·°C^{-1})	DC	direct current
k_r	radial thermal conductivity of battery (W·m^{-1}·°C^{-1})	DSC	differential scanning calorimetry
k_{r1}, k_{r2}	experimental and numerical radial thermal conductivity of battery (W·m^{-1}·°C^{-1})	EV	electric vehicles
k_{tim}	thermal conductivity of the interfacial thermal material (mm) (W·m^{-1}·°C^{-1})	LFP	lithium-iron phosphate
k_z	axial thermal conductivity of battery (W·m^{-1}·°C^{-1})	NCM	nickel cobalt manganese
L	layer thickness of the interfacial thermal material (mm)	OCV	open-circuit voltage
q	volumetric heat generation rate of the cylinder model (W·m^{-3})	SOC	state of charge
q_{ht}	heating power (W)	TR	thermal runaway
q''_{loss}	heat dissipation power (W·m^{-2})		
q_{in}	net heat flux density input to the lateral side of the battery (W·m^{-3})	*Greek symbols*	
q_{loss}	heat flux density lost on the outer surface (W·m^{-3})	α,β,γ	the coefficients to be determined
Q	heat generation (W)	λ_n	the characteristic value
$Q(t)$	heat flux generated by the cylinder (W)	θ	the temperature rise (°C)
Q_v	volumetric heat generation (W)	θ_{avg}	the average temperature rise (°C)
R	a cylinder with a radius (mm)	ρ	the density of the battery (kg·m^{-3})
R_f^2	the fitting coefficients	ρ_w	the density of water (kg·m^{-3})
$R_{z,b}$, $R_{r,b}$	axial and radial thermal resistance with heat source (°C·W^{-1})		
R''_{tim}	specific thermal resistance of the interface material (°C·m^2·W^{-1})	*Subscripts*	
Scalib	calibrated sensor sensitivity (μV·m^2·W^{-1})	*amb*	the ambient temperature
t	time (s)	r	the radial direction
T	temperature (°C)	*tim*	the interfacial thermal material
T_{amb}	environment temperature (°C)	z	the axial direction

1. Introduction

Lithium-ion batteries have been widely exploited as the power sources in electric vehicles, yet application issues concerning the thermal safety remain unsolved [1]. For instance, excessively high temperature can threaten the reliability and safety of the batteries in operation, whereas the issues of temperature non-uniformity significantly affect the whole lifetime of the battery system. Thermal safety and temperature control of the batteries are closely related to their thermophysical properties including the thermal conductivity and specific heat [2]. The thermal conductivity of batteries reflects their internal thermal conduction capability, affecting the temperature uniformity. The specific heat reflects the capability of the battery to absorb or release heat power per unit time and unit mass [3], affecting the temperature-rising rate and magnitude. Subsequently, it further affects a series of thermal effects generated by the battery. As such, accurate measurement of thermophysical parameters plays a crucial role in predicting their thermal behavior and preventing thermal runaway [4,5].

A number of research efforts have been devoted to the determination of battery thermophysical properties including the thermal conductivities and specific heat to address the aforementioned issues, which can be categorized into ex-situ and in-situ measurements [6]. Ex-situ measurement is defined to measure the thermal parameters of the respective components with the battery dismantling. Turner et al. [7] examined the components of the lithium-iron phosphate (LFP) battery by disassembly. The thermal conductivities were derived by the weighted average method, which were calculated as 1.79 W m^{-1} K^{-1} for the cathode and 1.17 W m^{-1} K^{-1} for the anode. Yang et al. [8] analyzed the major components of the battery and measured the thermal conductivity, which was estimated by fixing the sample with upper and bottom copper blocks. The significant impact of separators on the thermal conductivity was identified based on ex-situ measurements. Ponnappan et al. [9] measured the thermal conductivity of batteries by characterizing the contact resistances and obtaining the weighted average. The specific heat was also attained based on the ex-situ measurement. Loges et al. [10] employed differential scanning calorimetry (DSC) to investigate the specific heat of various components of seven types of prismatic and one type of pouch battery, involving the electrodes, separators, electrolytes, carbon-coated materials, with the set temperature range fluctuating from −40 to 60 °C. It was indicated that the battery specific heat increased with the increase in temperature, but insensitive to the state of charge (SOC). However, since the battery must be dismantled during the ex-situ measurement process, the deviations between the initial and dismantled assembly conditions such as stress states, and evaporation and overflow of the electrolyte could easily occur, causing inestimable impacts on parameter measurements. These deviations could introduce significant uncertainty into the measurement results obtained inherent in the ex-situ methods. Additionally, the exposure of the chemical substances in air could incur additional side reactions triggering hazardous risk such as fire and explosion. Due to the various factors influencing the measurement accuracy of the thermal conductivity, in-situ measurements are necessitated for the accurate measurement.

Among the in-situ measurements of thermal conductivities, Drake et al. [11] measured the thermophysical properties of 18650 batteries under quasi-steady heating condition, obtaining axial thermal conductivity of 30.4 W m^{-1} K^{-1} and radial thermal conductivity of 0.2 W m^{-1} K^{-1}. Sheng et al. [12] experimentally investigated the radial thermal conductivity of LFP prismatic batteries under a quasi-steady state condition, which was found to be 0.5 W m^{-1} K^{-1} at ambient temperature, increasing as the SOC increased slightly. Wu et al. [13] considered the anisotropy of thermal conductivities of 21700 batteries under quasi-steady condition, obtaining the axial and radial thermal conductivities of 24.2 W m^{-1} K^{-1} and 0.9 W m^{-1} K^{-1}, respectively. Wu et al. [14] studied the radial thermal conductivity of 32650 nickel cobalt manganese (NCM) batteries using the hot disk device under thermal runaway (TR) conditions within a thermostatic temperature range of 20 °C–120 °C. It was found that the radial thermal conductivity ranged from 1.738 to 2.358 W m^{-1} K^{-1}, first decreasing and then increasing with temperature. Feng et al. [15] used ARC to conduct TR test for a large-format prismatic battery and examined the fluctuation of the thermal parameters before and after the TR. It is found that, after TR, the specific heat decreased from 1090.2 J kg^{-1} K^{-1} to 1065.7 J kg^{-1} K^{-1}, whereas the anisotropic thermal conductivities in axial and radial direction decreased steeply from 15.9 to 0.548 W m^{-1} K^{-1} to 8.17 and 0.335 W m^{-1} K^{-1}, respectively.

In the thermal conductivity measurement, the heat flow should be carefully characterized since it is directly related to the measurement accuracy. Muhammad et al. [16] examined a method for obtaining the radial thermal conductivity of 0.39 W m^{-1} K^{-1} for 26650 cylindrical batteries, which considered the temporal variation of the heat flux entering the cylinder. Wang et al. [17] measured the thermal conductivities of prismatic batteries in the thickness direction and different discharge rates. It was found that the normal thermal conductivity varied at different positions in the battery large surface, with 2.27 W m^{-1} K^{-1} in the middle area and 3.19 W m^{-1} K^{-1} in the areas near the terminals. Huang et al. [18,19] focused on measuring the axial and radial thermal conductivities of NCA18650 cylindrical power batteries. Although the thermal conductivity measurement was considered one-dimensional steady-state conduction with lateral heat loss, the radial thermal conductivity measurement was more complex involving the matching of three-dimensional computational fluid dynamics (CFD) simulation by comparison with experimental data, which was time-consuming. While the existing studies more focus on a certain thermophysical parameters, there is lack of simultaneous determination of multiple parameters and dedicated heat flux regulation such as iso-flux condition, limiting the accuracy and applicability of the measurement results. Sheng et al. [20] considered the thermal conductivity anisotropy both of in the axial and radial directions for a cylindrical cell's core, which was obtained by fitting the three-dimensional numerical results against the experimental data. It was indicated that the anisotropy was inevitable, which had different influences in the prismatic and cylindrical batteries. Despite the increasing efforts on the anisotropy of thermal conductivity, there exist data scattering and inconsistency in the radial and axial thermal conductivities for different battery types. The differences could be attributed to interwined anisotropic heat flow and heat loss effects associated with the test methods, together with the variations in key battery components including the separator, cathode and anode materials, and electrolyte [21].

As against the dispersed results arising from the thermal conductivity measurements, the specific heat test results of different batteries followed a more normalized distribution, concentrated around the mean specific heat with a tolerable deviation [6]. Simultaneous determinations of multiple thermal parameters in a single test are also called for to minimize the test time and efforts. Since the ex-situ method may affect the status quo of the battery as has been mentioned, we mainly focus on in-situ measurements of specific heat for purpose of determining the multiple thermal parameters simultaneously. Accelerating rate calorimeter (ARC) had been utilized as the in-situ measurement. The use of ARC would create a nearly adiabatic chamber for maintaining the test battery with a smooth temperature rise which is related to the battery heating power and specific heat. Wang et al. [22] used the ARC measurement method to measure the specific heat of 18650 battery to be 935 J kg^{-1} °C^{-1} under a constant heating power of 0.7 W at approximately 45 °C. The specific heat influences with respect to the ambient temperature on the measurement results were also investigated, which could increase from 6 % [23] to 38 % [24] within temperature range −5 °C–55 °C, respectively. It should be pointed out that it is difficult to achieve an ideally adiabatic environment with unavoidable heat loss. Quasi-steady state tests have been studied by Drake et al. [11], who measured the specific heat of a 26650 battery with 1605 J kg^{-1} °C^{-1} regardless of the heat loss. Yu et al. [25] found that the specific heat increased by 17.1 % for the SOC decreasing from 1 to 0. Zhang et al. [26,27] developed an calorimetric method of the specific heat regarded a battery heating process, unveiling the linear results dependence on temperature. Wu et al. [28] utilized the calibrated calorimetric method to obtain the specific heat of cylindrical batteries. By placing an insulating material made of aerogel on the battery surface, the heat loss can be minimized and the specific heat can be measured accurately with the heat loss calibration. Faber et al. [29] extended the method to measure the specific heat of 18650 and 21700 cylindrical batteries and pouch battery. As the batteries were cycled between the hot and cold thermostat chambers, the temperature-dependent specific heat can be obtained, which nonetheless requires a relatively long test time to obtain. In general, there is a lack of in-situ measurement studies for simultaneous determination of radial thermal conductivity and the specific heat for lithium-ion batteries warranting both accuracy and test efficiency, which still needs to be investigated.

In this paper, a novel approach is proposed for measuring the thermophysical properties of cylindrical batteries under a calibrated iso-flux condition. To reduce heat loss and maintain higher measurement accuracy, six protective batteries of the same model and brand number are placed around the test battery at the center, creating a nearly adiabatic environment with a calibrated iso-flux for the test battery to prevent adverse heat leakage from its lateral surface. The theoretical analysis is presented for the radial thermal conductivity and specific heat. Accurate fitting results are obtained by adopting the double exponential function for determining the specific heat, the fitting algorithm error of which (<0.1 %) could be neglected in the data reduction. In addition, the heat leakage from the lateral side is minimized, ensuring the iso-flux heat input to the test battery and thereby enabling simultaneous measurement of the specific heat and radial thermal conductivity of cylindrical batteries in a fast manner. Overall, this work contributes to the advancement of thermophysical property measurement techniques for cylindrical batteries, enabling accurate characterization of their thermal characteristics and corresponding thermal designs.

2. Theoretical analysis model

Considering the battery as a cylinder with a radius of R and thermal insulation at the two ends, its axial thermal conduction can be neglected whereas its lateral surface is subjected to a time-varying heat input by a thin film heater fully wrapped around at $r = R$.

The battery's lateral temperature rise and net heat flux entering the battery interior are used for quantitating the thermal parameters of the cylinder. Assuming the thermal conductivity, specific heat, and density of the battery are k, c, and ρ respectively, with the subscript r denoting the radial direction, the energy conservation equation for the temperature rise $\theta(r, t)$ within the battery subjected to the lateral heat input is given by the following equation [11]:

$$\rho c \frac{\partial \theta}{\partial t} = \frac{k_r}{r} \frac{\partial}{\partial r}\left(r \frac{\partial \theta}{\partial r} \right) \tag{1}$$

where $\theta(r, t) = T\text{-}T_{\mathrm{amb}}$, T represents the lateral temperature and t represents time, and the subscripts amb and r represent the ambient temperature and radial coordinate, respectively. Assuming that the heat flux entering the battery is $Q(t)$, where $Q(t)$ is the time-varying heat generation rate, the boundary condition applied at $r = R$ for the heating surface of the thin film heater is given by the following equation:

$$Q(t) = k_r \frac{\partial \theta}{\partial r} \quad at \quad r = R \tag{2}$$

At $r = 0$, the boundary condition is:

$$\frac{\partial \theta}{\partial r} = 0 \tag{3}$$

Considering that the initial temperature rise is zero, i.e., $\theta(\mathrm{r}, 0) = 0$. At this point, the final solution is a characteristic function containing time-dependent coefficients $c_{\mathrm{n}}(\mathrm{t})$, which can be obtained by applying the method of undetermined coefficients for Eqs. (1)–(3). The form of the solution is given as follows [16]:

$$\theta(r, t) - \theta_{avg}(t) = \sum_{n=1}^{\infty} c_n(t) J_0(\lambda_n r) \tag{4}$$

$$\theta_{avg}(t) = \frac{2 \int_0^t Q(t) dt}{\rho c R} \tag{5}$$

where J_0 represents the zeroth-order Bessel function of the first kind, and the characteristic values λ_n are obtained from the roots of J_1, which is the first-order Bessel function of the first kind. θ_{avg} is the average temperature rise.

For the special case that $Q(\mathrm{t}) = Q$ is constant, by substituting Eq. (4) into Eq. (1) and simplifying it using the boundary conditions Eq. (2), the battery temperature rise $\theta(r, t)$ is obtained as:

$$\theta(r,t)=\frac{2Qt}{\rho cR}+\frac{Q}{k_rR}\left(\frac{r^2}{2}-\frac{R^2}{4}\right)-\frac{2QR}{k_r}\sum_{n=1}^{\infty}\frac{J_0\left(\lambda_n\frac{r}{R}\right)}{\lambda_n^2J_0(\lambda_n)}e^{-\frac{k_r\lambda_n^2}{\rho cR^2}t} \tag{6}$$

Furthermore, Eq. (6) can be expressed as a function of the Fourier number Fo to further simplify it, where $Fo = kt/(\rho cR^2)$. According to the transient heat transfer results with the iso-flux condition, when Fo is around or less than 0.2, the approximate solution for the radial thermal conductivity is:

$$k_r=\frac{8q_{in}R}{\left(4\sqrt{\frac{\pi}{Fo}}-\pi\right)\Delta T} \tag{7}$$

where ΔT represents the average temperature rise of the lateral side of the battery. It can be observed that Eq. (7) correlates the radial thermal conductivity with the Fourier number Fo. By solving Eq. (7), we can obtain an analytical solution for the radial thermal conductivity in term of ΔT and t:

$$k_r=\frac{8\left(-\sqrt{\Delta T(\rho cR\Delta T-2q_{in}t)\rho cR}+\rho cR\Delta T-q_{in}t\right)R}{\pi t\Delta T} \tag{8}$$

where q_{in} is the net heat flux density input to the lateral side of the battery, given by $q_{in} = Q/(2\pi RH)$ - q_{loss}, with q_{loss} representing the heat loss flux from the outer surface. Then, the battery's specific heat can be expressed in terms of the temperature rise rate dT/dt during the quasi-steady state as:

$$c=\frac{2q_{in}}{\rho R\frac{dT}{dt}} \tag{9}$$

As mentioned above, the formula for solving the radial thermal conductivity is valid when Fo is within 0.2 for idealized cylinder heated from the lateral surface. For the battery subjected to the heating of film heater with thermal interface resistance, the time response could be prolonged and thus the Fo value based on the idealized cylinder model could be somewhat larger than 0.2, which will be elaborated in the later section. The procedural steps outlined in this paper for the solution are illustrated in Fig. 1.

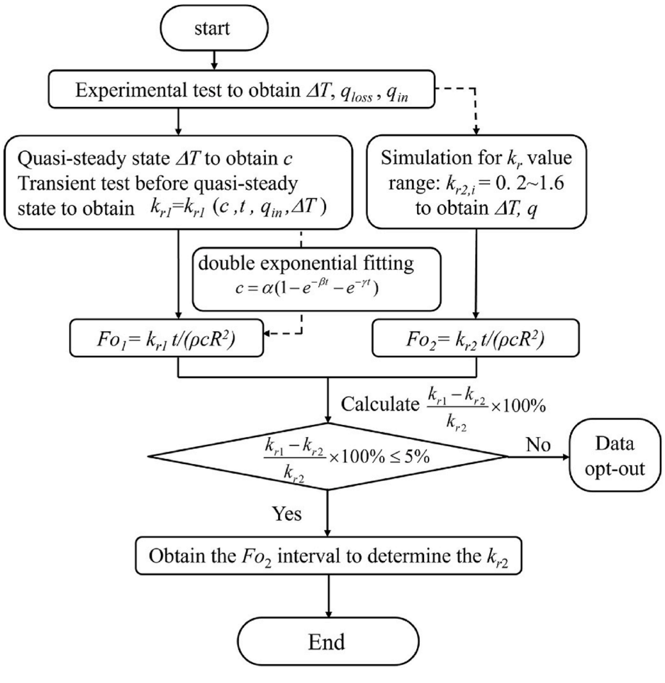

Fig. 1. Flowchart for solving specific heat and radial thermal conductivity.

3. Experimental study

3.1. Calibrated iso-flux experiment

In this paper, the 18650 ternary lithium-ion battery by LG Co. was used as the test battery to elaborate the in-situ measurement of the radial thermal conductivity as well as the specific heat. The specifications of the battery are given in Table 1. For the single battery, its radial thermal conductivity was tested at the ambient temperatures ranging from −15 to 45 °C, with a heating power of 1.93 W for the test battery at the center.

The experimental setup for measuring the thermophysical properties of the test batteries is shown in Fig. 2. The setup included a temperature-controlled chamber, a battery pack placed inside the chamber, heating components for temperature elevation, and a data acquisition and processing unit for measuring the temperature of the batteries. Seven batteries were fixed together in the collars of two 3D-printed sleeves. The thin film heater was connected to a GWINSTEK GPD-2303S DC power supply to provide an iso-flux input to the battery. The thermocouples monitoring the battery surface were connected to an Agilent data acquisition instrument, with a data acquisition interval of 1 s. Additionally, thermally conductive silicone grease (model HM-712N) was applied to the circumference surface between the batteries and the thin film heaters, which had the thermal conductivity of 2.38 W m^{-1} $°C^{-1}$. By heating the lateral sides of the test battery and the surrounding batteries simultaneously, the heat flux q_{in} was maintained under calibrated iso-flux condition, while the heat loss rate was controlled at a minimum level. Considering the transient temperature rises of the outer surface, the specific heat and radial thermal conductivity of the cylindrical battery could be obtained. Therefore, this method enabled non-destructive measurement of the specific heat and radial thermal conductivity of cylindrical batteries under different temperature conditions.

The experimental procedures are described as follows. First, seven batteries were placed on a charge-discharge tester and subjected to a 0.5C (rate of charge/discharge) charge-discharge cycle to be activated, ultimately resulting in all the seven batteries with the same SOC (100 %). Three T-type thermocouples (wire diameter 0.1 mm, National Level 1 accuracy) were welded to the upper, middle, and bottom of the test battery, evenly distributed around the peripheral, to measure the real-time temperature changes. A high thermal conductivity graphite sheet, which had an adhesive layer, is attached between the cylindrical battery and the thin film heater to uniformize the heat flux entering the battery. Notably, as pointed out in the previous work [2], the deviation in calculating the specific heat could be as high as 10.70 % if without using the graphite sheet. A layer of thermally conductive silicone grease was evenly applied to the thin film heaters to eliminate contact thermal resistance with the batteries. A heat flux sensor, with the model No. of HFS-5 produced by OMEGA, was attached to the surface center of the central battery to quantitatively monitor the heat dissipation from the

Table 1
Basic parameters of the 18650 batteries.

Parameter (unit)	value	Parameter (unit)	Value
Nominal capacity (Ah)	2.5	Anode	Ni-Co-Mn 523
Nominal voltage (V)	3.6	Cathode	Graphite
Charge cut-off voltage (V)	4.2	Battery mass (g)	45.5
Discharge cut-off voltage (V)	2.5	Battery length (mm)	65
Maximum charge current (A)	4	Battery diameter (mm)	18.2
Maximum discharge current (A)	30	Density (kg·m^{-3})	2690
Standard charge current (A)	1.25	Testing ambient temperature (°C)	−15~45
Charge cut-off current(A)	0.2	Heating power (W)	1.93
Electrolyte material	$LiPF_6$		

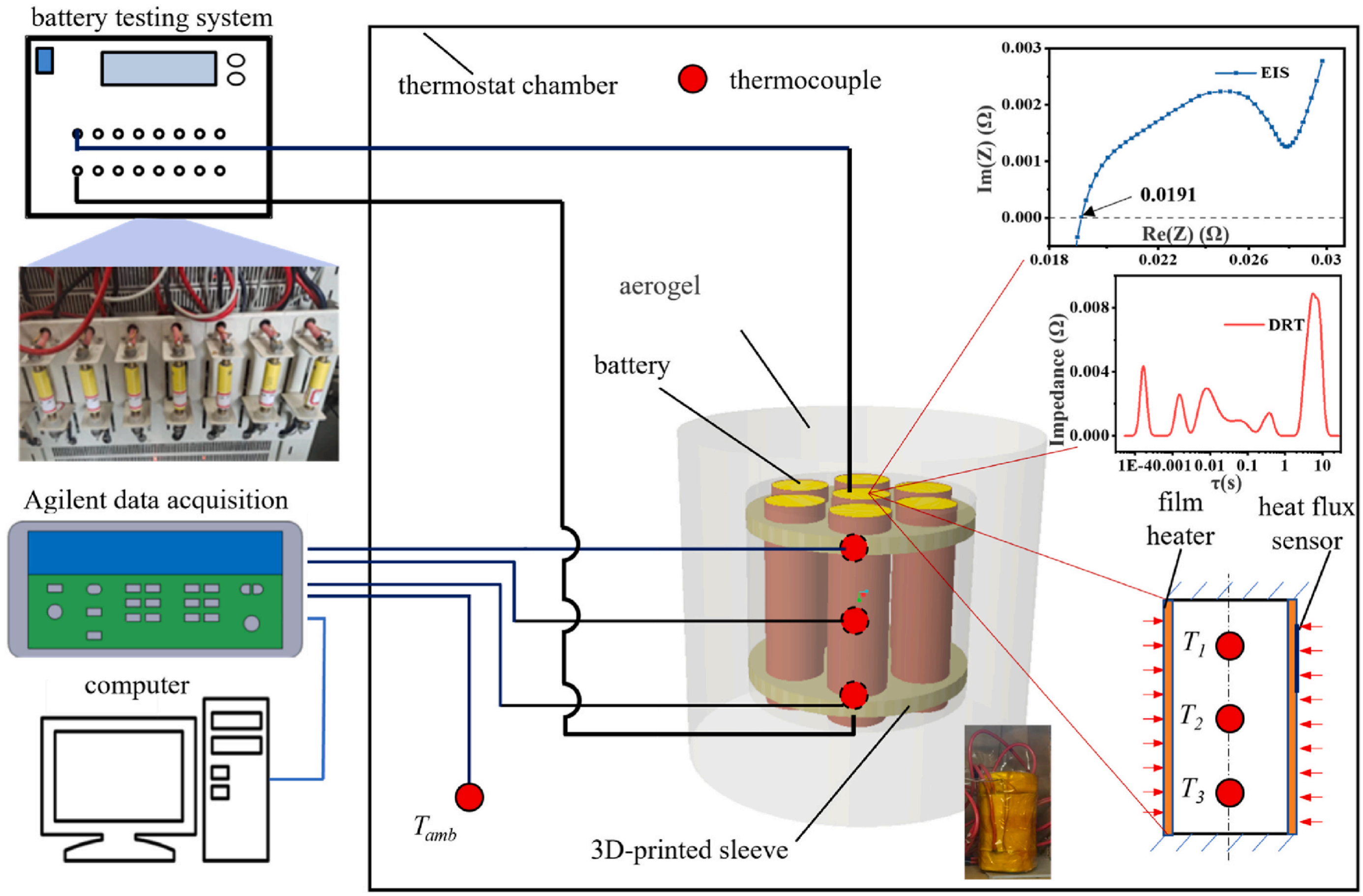

Fig. 2. Experimental setup for calibrated iso-flux condition, together with the electrochemical impedance spectroscopy and thermocouple locations on the battery at the rightmost side.

test battery. After the thin film heaters were affixed to all the batteries including the six surrounding batteries, the seven batteries were fixed up with upper and lower collars with a battery-to-battery gap around 2 mm, which were then wrapped around with 20 mm thick aerogel insulation made of silicon oxide. Aerogel powders could be added in between the battery gaps to enhance the insulation. The assembled test setup was placed in a temperature-controlled chamber, and film heater was connected to the DC power supply, whereas the wires of the thermocouples, among others, were led outside to connect Agilent data acquisition instrument. By adjusting the initial temperature of the temperature-controlled chamber, the radial thermal conductivity and specific heat could be measured at different ambient temperatures during these experiments.

In the product specification sheet of LG18650 battery, the battery alternative-current impedance $\leq$20 mΩ at 1 kHz after charge at 23 °C ± 2 °C is considered qualified. In this work, a CHT3563A precision impedance analyzer was applied to measure the alternative-current impedance, and the result was 19.2 mΩ at the open-circuit voltage (OCV) of 4.07 V. We also used electrochemical impedance spectroscope to extract the respective impedances by distribution-of-relaxation-times analysis [30]. We found that the ohmic resistance, solid electrolyte interphase impedance, charge transfer impedance and diffusion impedance were 4.374 mΩ, 2.587 mΩ, 2.991 mΩ and 8.919 mΩ, respectively. A sum of the four impedances led to a total impedance of 18.9 mΩ, which agrees with the impedance analyzer result within 1.7 %. As such, the present battery was used as the test battery for the thermal parameter test.

3.2. *Experiment for heat flux calibration*

The experimental setup for the heat flux sensor calibration experiment is shown in Fig. 3(a). A simulated cylindrical battery made of aluminum shell with internal heating rod was employed to provide the heating power. A graphite sheet layer was adhered to the heating rod's surface to ensure uniform temperature distribution on its exterior. A T-type thermocouple was installed on the simulated battery for temperature change monitoring. A thin layer of thermally conductive silicone grease was evenly applied to the interface with the heat flux sensor against the test battery for reducing the contact thermal resistance. Then, the heat flux sensor was attached to the center of the simulated battery surface and fixed with polyimide tape to monitor the heat flow from the battery to the external environment. Finally, to maintain heat retention, the simulated battery is enclosed with double layers of aerogel insulation blankets. The simulated battery was placed inside an acrylic box within a thermostatic temperature chamber controlled at the set temperature such as 25 °C to maintain stable natural convection of the test section. The thermocouples and heat flux sensor were connected with an external Agilent data acquisition instrument to collect the output voltage and temperature signals. The two wires of the heating rod were connected to an external direct current (DC) power supply to provide the required power for the experiment, which was 1.93 W in this work.

Once the simulated battery temperature reached the steady state, the heating power and the voltage of the heat flux sensor were recorded to obtain the calibrated sensor sensitivity. Fig. 3(b) depicts the heat dissipation power over time after reaching the steady state during the experiment. At this stage, the heat dissipation power is equal to the

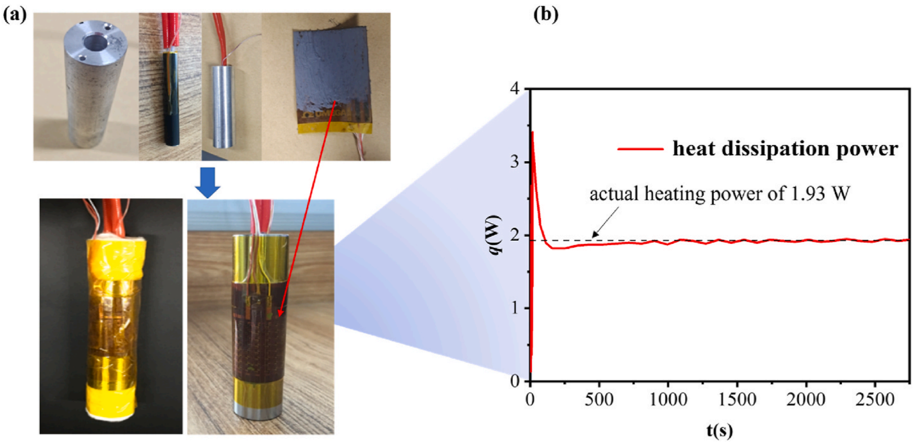

Fig. 3. (a) The heat flux sensor assembly diagram for the calibration experiment. (b) heat dissipation power with time as measured by the heat flux sensor vs the actual heating power of 1.93 W.

heating power q_{ht}, namely,

$$q_{ht} = q_{loss}{}'' A \tag{10}$$

$$q_{loss}{}'' = \frac{\Delta V}{[0.00334 \times T + 0.917] \times Scalib} \tag{11}$$

where A is the surface area of the test battery, ΔV is the heat flux voltage output in μV as read by the heat flux sensor, *Scalib* is the calibrated sensor sensitivity, which was identified to be 1.43 μV m^2 W^{-1} in this study.

4. Results and discussion

4.1. Battery transient thermal characteristics

The battery thermal conductivity results were obtained through a comparison of experiment and simulations at different temperatures. Fig. 4 presents the test results for the 18650 lithium-ion batteries at set temperatures of −15 °C, 5 °C, 25 °C, and 45 °C in a thermostatic temperature chamber. Fig. 4(a) shows the temperature rises of the battery at different ambient temperatures. The net heat flux value together with the heat loss to the ambient measured by the heat flux sensor is shown in Fig. 4(b). The net heat flux entering the lateral side of the battery stabilizes, and the temperature rise is within 15 °C. It is also identified that the heat flux would achieve iso-flux condition of 1.93 W at 40 s after the heating is started, which is within 3 % from the heating power input to the film heater. As such, the iso-flux of 445 W m^{-2} is used for the subsequent thermal parameter calculations.

Fig. 4(c) indicates that the slope and heat flux are substituted into Eq. (9) to obtain specific heat of 1043 J kg^{-1} °C^{-1} at this time, which increases slightly with the set temperature increasing. It is noted that the case at 45 °C ambient temperature only last for 306s when the battery

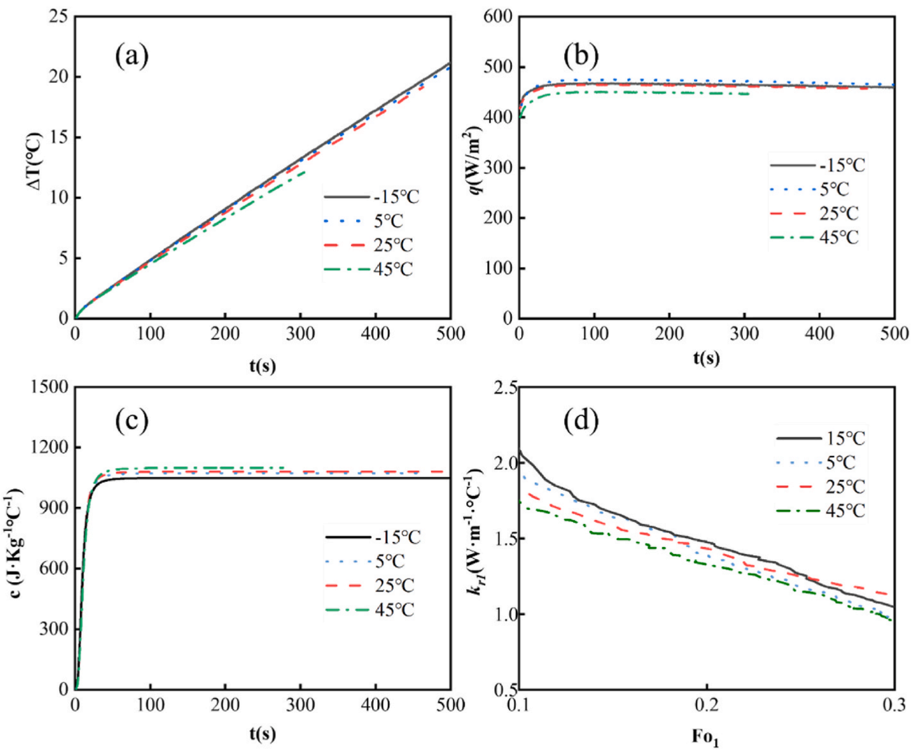

Fig. 4. Test results under different ambient temperatures: (a) temperature rise. (b) net heat flux. (c) specific heat. (d) radial thermal conductivity varying with Fo_1.

temperature reached the threshold of 60 °C, and thus the heating was stopped to minimize the thermal runaway risk. In the data reduction, the specific heat can also be attained based on the fitting of the double exponential function as follows:

$$c=\alpha\left(1-e^{-\beta t}-e^{-\gamma t}\right)\begin{cases}\alpha=987.2 \quad \beta=0.0867 \quad \gamma=1.3613 \quad T=-15^{\circ}C\\ \alpha=1017.3 \quad \beta=0.0844 \quad \gamma=1.3354 \quad T=5^{\circ}C\\ \alpha=1044.4 \quad \beta=0.0842 \quad \gamma=1.4090 \quad T=25^{\circ}C\\ \alpha=1076.3 \quad \beta=0.0758 \quad \gamma=1.2450 \quad T=45^{\circ}C\end{cases} \tag{12}$$

where α, β, γ representing the coefficients to be determined. We also compare the fitting results using the shorter time data between 0 and 300s in comparison with those using the longer time data between 0 and 500s based on the fitting method as given in Eq. (12) for all the ambient temperature cases except T = 45 °C. The comparison indicates that the difference between two specific heats obtain from the above two algorithms with different time intervals was less than 0.1 %, with the fitting coefficients of R_f^2 values all above 95 %. As such, the fitting errors could be neglected in the data reduction for determining the specific heat based on the double exponential function fitting. Ultimately, the specific heats are determined to be 987.2, 1017.3, 1043.4 and 1076.3 J kg^{-1} °C^{-1}, respectively, at the set temperatures of −15 °C, 5 °C, 25 °C, and 45 °C. It should be noted that the use of a single exponential function may produce a fitting coefficient of R_f^2 around 70 %, which is not sufficient to ensure a small error level.

Based on the specific heat values determined by Eq. (12), one can calculate the experimentally determined instantaneous thermal conductivity k_{r1} (t) as it varies over time. Fig. 4(d) displays the radial thermal conductivity calculated based on the experimentally measured temperature rise at the lateral side under the calibrated heat flux condition, plotted against the Fourier number. When the radial thermal conductivity ranges from 1.0 to 1.8 W m^{-1} °C^{-1}, the corresponding Fourier number Fo_1 values are between 0.10 and 0.30. The determination of the k_r will be analyzed in the later section in conjunction with the numerical simulation results under the same boundary conditions.

4.2. Numerical simulation and thermal parameter determination

In the simulation work, the following assumptions have been made.

- The battery is assumed as homogeneous anisotropic solid with thermally insulated end terminals, except for the heating flux on the lateral cylinder surface.
- The constant heat flux from the film heater by eliminating the minimal heat loss to the ambient is directly applied on the surface of the battery without considering the film heater and the graphite sheet in between due to the minimal thermal effects therein.
- The heat loss due to the thermocouple connections is neglected.

The experimentally calculated transient thermal conductivities k_{r1} are divided into intervals based on its numerical range, assuming k_{r1} falls within the range of 0.2–3.0 W m^{-1} °C^{-1}. Then, based on each input value of k_{r2} (0.2, 0.4, 0.6, 0.8, 1, 1.2, 1.4, 1.6, 3.0 W m^{-1} °C^{-1}), the specific heat c, and the net heat flux q, a 1:1 one-dimensional thermal conductivity model is established for a single battery to conduct numerical simulations. 1.93 W from 0 to 500 s is taken as the net heat flux input for the battery value of specific heat simulation. A mesh with 1472 cells is sufficient for the one-dimensional model, which may take only 3~4 min to complete based on a notebook computer with 32 GB memory and AMD Ryzen 7 CPU. The temperature rise of the battery obtained from the simulation is denoted as ΔT_2. Based on the measurement results in Fig. 4, a numerical simulation model of a single battery under the same heat flux boundary condition as the experiment is established. The relevant parameters of simulation are provided in Table 2.

Table 2
Parameters for single-battery numerical simulation model.

Parameter (unit)	18650 batteries
Ambient temperature (°C)	25
Density (kg·m^{-3})	2690
Battery mass (g)	45.5
Battery length (mm)	65
Battery diameter (mm)	18.1
Convective heat transfer coefficient (W·m^{-2}·°C^{-1})	0
Specific heat (J·kg^{-1}·°C^{-1})	1043 (this study)
Axial thermal conductivity (W·m^{-1}·°C^{-1})	15.23 [2]
Radial thermal conductivity(W·m^{-1}·°C^{-1})	0.2–3.0

The measured heat flux boundary condition q_{in} is utilized as the lateral boundary condition for the numerical simulation. Simulations for different input values of k_r are conducted to obtain their respective battery temperature rises ΔT_2. Fig. 5(a) shows the simulation results of the single battery at 25 °C. To facilitate experimental measurements, the range of Fourier numbers corresponding to the relative error (k_{r1}-k_{r2})/k_{r1} $\leq$ 5 % (Fig. 2) is taken as the final data processing segment for determination of the radial thermal conductivity. This has been encircled in the middle region in Fig. 5(b). The minimum Fo_2 value of 0.233 is obtained when $k_{r2} = 3.0$ W m^{-1} °C^{-1} at the leftmost end of the encircled region, and the maximum Fo_2 value of 0.266 is obtained when $k_{r2} = 0.2$ W m^{-1} °C^{-1} at the rightmost end of the encircled region. In other words, the corresponding Fo range with the minimal error falls between 0.233 and 0.266, with a relative error of 6.0 %. The thermal conductivity k_{r2} calculated within the Fo range of 0.233–0.266 in Fig. 4(d) is averaged, and the radial thermal conductivity of the battery is determined with the weighted average method in Ref. [17]. As such, the average value of 1.181 W m^{-1} °C^{-1} is the experimentally measured radial thermal conductivity.

The numerical simulations based on the experimentally-obtained thermal parameters are further conducted, which show the maximum relative error of 1.8 % in the maximum lateral temperature as against the experimental measurement. This further validates the accuracy of the measured radial thermal conductivity values obtained in this method.

4.3. Thermal parameters at different temperatures

Based on Figs. 1 and 5(b), it is noted that the average specific heat and radial thermal conductivities of the test battery are calculated from −15 °C to 45 °C. Fig. 6 displays the fitting curves of specific heat and thermal conductivity. It indicates that the specific heat can be fitted into a linear curve with the set temperature of the thermostatic temperature chamber, and the reliability of the fitting formula is as high as 99.8 %. The specific heat of the cylindrical battery increases from 987.2 to 1076 J kg^{-1} °C^{-1}, with the temperature increasing from −15 °C to 45 °C, representing an increase of approximately 9.02 % over the temperature range or 0.15 % per °C. The radial thermal conductivities of the battery are plotted in Fig. 6 based on the set results of the thermostatic temperature chamber. It is seen that the radial thermal conductivities of the battery range from 1.147 to 1.250 W m^{-1} °C^{-1} at the set temperatures of −15 °C, 5 °C, 25 °C, and 45 °C, representing an increase of 8.99 % or similar increasing trend with temperature at the rate around 0.15 % per °C.

4.4. Experimental uncertainty analysis

The uncertainty in radial thermal conductivity measurements can be ascribed to the uncertainty of the measurement setup and random fluctuations. Random fluctuations can be minimized by conducting multiple measurements and averaging them during battery mass testing processes. Due to the excellent adiabatic environment properties of

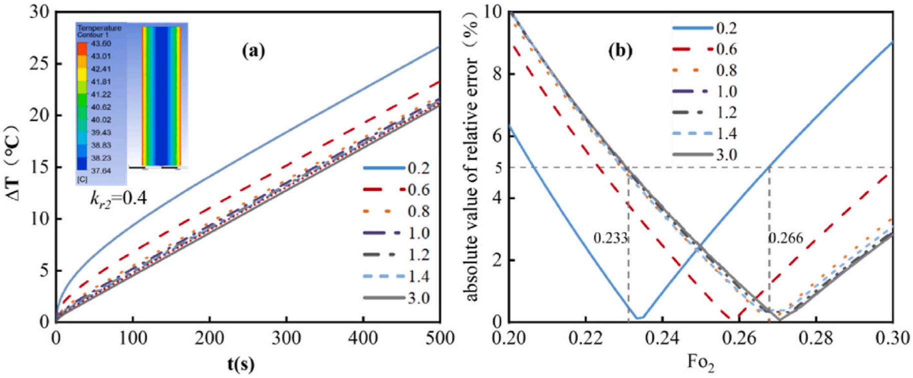

Fig. 5. Simulation results: (a) temperature rise $\Delta T = \Delta T_2$ diagram on the lateral side of the battery with different input radial thermal conductivities k_{r2}. (b) the absolute value of the relative error between the numerically simulated radial thermal conductivity and Fo_2 at 25 °C, and the suitable Fo_2 in the encircled region within minimal error 6.0 %.

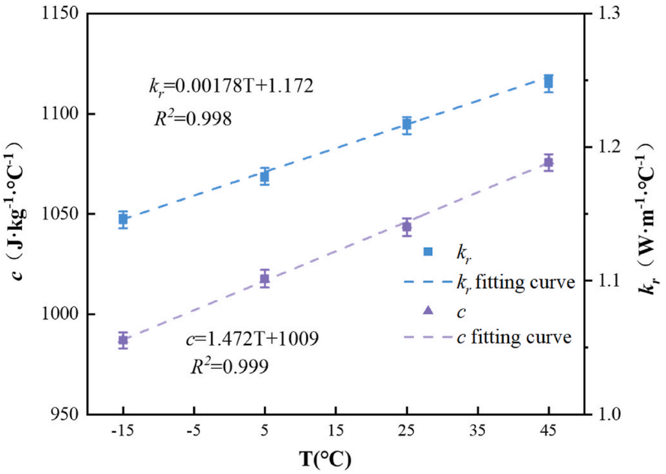

Fig. 6. Fitting results of specific heat and radial thermal conductivity varying with set temperature.

aerogel, the random fluctuation in the repeatability of the experimental test is found to be minimal around 0.2 %.

In this study, the uncertainty of the T-type thermocouple is estimated to be 1 % given the battery temperature rise of 20 °C. Additionally, the uncertainty of the dT/dt is estimated to be 1.42 % plus the fitting algorithm deviation of 0.1 %. The uncertainty of the data acquisition equipment is 0.3 %, while the electronic balance has the uncertainty of 1.0 %. Thus, the uncertainty of the specific heat for the test battery is estimated as follows.

$$\frac{\delta c}{c} = \sqrt{\left(\frac{\delta q_{in}}{q_{in}}\right)^2 + \left(\frac{\delta \rho}{\rho}\right)^2 + \left(\frac{\delta R}{R}\right)^2 + \left(\frac{\delta(dT/dt)}{dT/dt}\right)^2} \tag{13}$$

The uncertainty of the specific heat is calculated by approximately 3.5 %.

Subsequently, the uncertainty of the radial thermal conductivity is estimated as follows by taking into account the variations in Fourier number, density, specific capacity, time and radius. Namely Eq. (14).

$$\frac{\delta k_r}{k_r} = \sqrt{\left(\frac{\delta Fo}{Fo}\right)^2 + \left(\frac{\delta \rho}{\rho}\right)^2 + \left(\frac{\delta c}{c}\right)^2 + 4\left(\frac{\delta R}{R}\right)^2 + (\delta R_{random})^2} \tag{14}$$

For cylindrical lithium-ion batteries, the uncertainty of the radial thermal conductivity is calculated by approximately 6.14 %. The uncertainty error bars for both radial conductivity and specific heat are also presented in Fig. 6.

4.5. Analysis of thermal management

The impact of the radial thermal conductivity of the 18650 cylindrical batteries as well as the newly developed 46800 batteries on the thermal management design is discussed in this section [31]. It is noted that the thermal management can be implemented with either bottom cooling or lateral side cooling, both of which are displayed in the inserts in Fig. 7. For example, in the liquid cooling thermal management, the velocity $v = 1$ m s^{-1} was set for the coolant, and the water temperature rise ΔT_{w} for bottom cooling is given by [32].

$$\Delta T_w = \frac{Q_v}{\rho_w A_w v c_w} \tag{15}$$

where Q_v represents the volumetric heat generation when the battery operated at a high discharge rate such as 3C, ρ_{w} represents the density of water, A_w the cross-sectional area of cooling channels, and c_{w} the specific heat of coolant water. It is noted that the water temperature increases by 0.063 °C when the battery operated at 3C ($Q_v = 1.79$ W), which is ignored for the present thermal analysis. The maximum temperature rise ΔT_{z} for the bottom cooling is written as [33].

$$\Delta T_z = T_{\max} - T_{out} = Q_v\left[R_{z,b} + R_{tim}'' / \left(\pi R^2\right)\right] \tag{16}$$

$$R_{z,b} = \frac{1}{2}\frac{H}{k_z \pi R^2} \tag{17}$$

where $T_{\max}$ and T_{out} are the maximum battery temperature and cold plate temperature, H is height of the battery, $R_{\mathrm{z,b}}$ is the axial thermal resistance with heat source [33], R_{tim}'' is the specific thermal resistance between the cold plate and the battery, and the subscripts z and tim denote the axial direction and interfacial thermal material, respectively. The specific thermal resistance of the interface material is normally made of silicone sponge with thermally conductive filers as described in Ref. [34], $R_{tim}'' = L/k_{tim}$, with L and k_{tim} the thickness and thermal conductivity of the thermal interface material, respectively. The maximum temperature rise ΔT_{r} for the lateral cooling is expressed as

$$\Delta T_r = T_{\max} - T_{out} = Q_v\left[R_{r,b} + R_{tim}'' / (2\pi RH/3)\right] \tag{18}$$

$$R_{r,b} = \frac{1}{4\pi k_r H} \tag{19}$$

where $T_{\max}$, T_{out} and R_{tim}''have been defined above, $R_{\mathrm{r,b}}$ is the thermal resistance of the battery in the radial direction.

Assuming the 60° contact angle [35] and thus 1/3 circumference area of the battery contacting the serpentine tube, the resulting effective interfacial thermal resistance is obtained for the calculation of the temperature rise. We use the maximum temperature ratio between the lateral side cooling and bottom cooling to evaluate the performance by

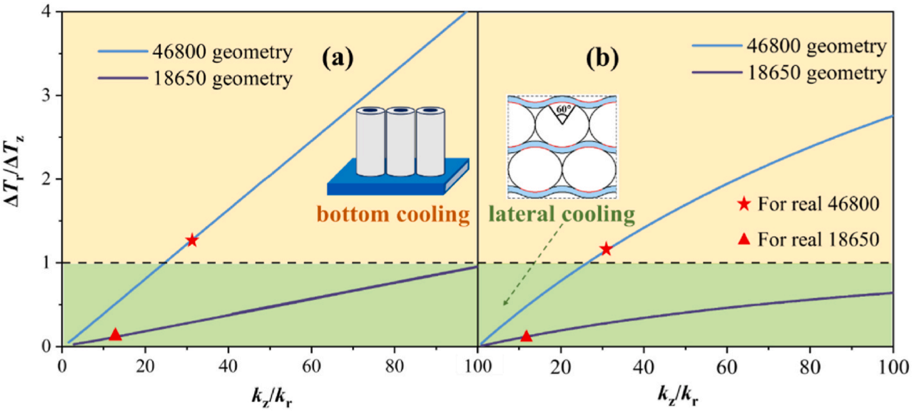

Fig. 7. 18650 and 46800 battery types comparison with bottom cooling and lateral cooling based on the $\Delta T_r/\Delta T_z$ vs k_z/k_r (a) without and (b) with the interfacial thermal resistance.

dividing Eq. (18) with Eq. (16). Namely

$$\frac{\Delta T_r}{\Delta T_z} = \frac{R_{r,b} + R_{tim}''/(2\pi RH/3)}{R_{z,b} + R_{tim}''/(\pi R^2)} = \frac{R^2 + 6Rk_rR_{tim}''}{2H^2k_r/k_z + 4Hk_rR_{tim}''} \tag{20}$$

Considering the use of the same interfacial thermal material with the layer thickness of $L = 0.5$ mm and thermal conductivity of $k_{tim} = 1.5$ W $\text{m}^{-1}\,^\circ\text{C}^{-1}$, we can obtain $R_{tim}'' = 1 \times 10^{-3}\ ^\circ\text{C}\cdot\text{m}^2\cdot\text{W}^{-1}$ for both cooling cases. It is noted that the bottom cooling is preferred when the ratio $\Delta T_r/\Delta T_z > 1$, whereas the lateral cooling is preferred when the ratio $\Delta T_r/\Delta T_z < 1$.

The ratios of the maximum temperature rise for 18650 and 46800 types of batteries in the radial and axial directions are plotted in Fig. 7, as against k_z/k_r, the ratio of axial and radial thermal conductivity. Note that the radial thermal conductivity of the 46800 battery takes the same k_r value of 1.181 W $\text{m}^{-1}\,^\circ\text{C}^{-1}$ as tested for the present 18650 battery due to the similar rolling process. However, the 46800 thermal conductivity in the axial direction has been much improved than the conventional tabbed design since the tabless 46800 design eliminates the tab resistance. As such, the $k_z = 36.96$ W $\text{m}^{-1}\,^\circ\text{C}^{-1}$ based on the electrode material as tested by Maleki et al. [36] is used. The calculation shows that, for the real 18650 battery as measured in the present study, the temperature rise ratio of $\Delta T_r/\Delta T_z$ is less than 1 for the slim 18650 geometry model. As such, the lateral side cooling is more efficient than the bottom cooling for the 18650 batteries, either with or without the thermal interfacial material. On the other hand, the temperature rise ratio is larger than 1 when the k_z/k_r is larger than 27 with the thermal interfacial material or 25 without the interfacial material for the plump 46800 geometry. For the real 46800 with $k_r = 1.181$ W $\text{m}^{-1}\,^\circ\text{C}^{-1}$ and $k_z = 36.96$ W $\text{m}^{-1}\,^\circ\text{C}^{-1}$, the temperature rise ratio is 31.29, as indicated by the pentagon symbol in Fig. 7, and thus the bottom cooling is more effective for this battery format. As such, the present measurement could provide fundamental thermal parameters for the effective thermal management of batteries with ever-evolving sizes and formats.

Similar to the cylindrical battery, large-size prismatic batteries also exhibit the anisotropy in the thermophysical properties in the thickness and width directions. The research philosophy and algorithm outlined in this paper basically can be extended to the prismatic batteries, with some aspects that require slight adjustments. The boundary conditions could be calibrated as iso-flux condition with the similar thermal protection method in our work. The fitting model for specific heat would remain the same, and the thermal conductivity model could be implemented for flat plane heat conduction by referring to the textbook [37].

5. Conclusion

This study reports a novel method for measuring the radial thermal conductivity and specific heat of 18650 cylindrical lithium-ion batteries under calibrated iso-flux condition in combination with the one-dimensional simulation. By arranging six batteries surrounding a test battery at the center and heating the batteries from the lateral side, a calibrated iso-flux environment is created for the test battery. Based on transient and quasi-steady state heat conduction theories, the methods for simultaneously determining the specific heat and radial thermal conductivity of the battery are developed with augmented accuracy in a fast manner. The specific heat can be directly obtained by double exponential fitting of the experimental data (~0.1 % in algorithm error), whereas the radial thermal conductivity of cylindrical lithium-ion batteries is obtained by minimizing the deviations between the measurement and the one-dimensional simulation model. It is indicated that, as the set temperature is increased from −15 °C to 45 °C, both of the specific heat and radial thermal conductivity increase almost linearly with temperature. Finally, a comparative analysis of different cooling methods is conducted on the thermal management of batteries in both slim 18650 and plump 46800 formats. It is identified that the slim 18650 batteries configured with the lateral side cooling have smaller temperature rises, whereas the plump 46800 real batteries with the bottom cooling have smaller temperature rises. Obviously, accurate determination of the thermal parameters in the present work could benefit thermal analysis of battery thermal management and help to optimize the design configurations.

CRediT authorship contribution statement

Ruitong Liu: Writing – original draft, Methodology, Investigation, Conceptualization. **Hengyun Zhang:** Writing – original draft, Investigation, Funding acquisition, Formal analysis, Conceptualization. **Jinqi Liu:** Writing – review & editing. **Hong Yu:** Writing – review & editing. **Shen Xu:** Writing – review & editing. **Xinwei Wang:** Writing – review & editing.

Declaration of competing interest

This work was supported by the National Natural Science Foundations of China (52476079) and Shanghai Municipal Natural Science Foundation (21ZR1426300).

All authors have approved the manuscript and agree with its submission to Journal of Power Sources.

All authors declare that there are no conflicts of interest or competing interests regarding the publication of this manuscript.

Acknowledgement

This work was supported by the National Natural Science Foundations of China (52476079) and Shanghai Municipal Natural Science

Foundation (21ZR1426300).

Data availability

Data will be made available on request.

References

[1] X. Feng, M. Ouyang, X. Liu, et al., Thermal runaway mechanism of lithium-ion battery for electric vehicles: a review, Energy Storage Mater. 10 (2018) 246–267, https://doi.org/10.1016/j.ensm.2017.05.013.

[2] H. Yu, H. Zhang, J. Shi, et al., Thermal parameters of cylindrical power batteries: quasi-steady state heat guarding measurement and thermal management strategies, Appl. Therm. Eng. 231 (2023) 120959, https://doi.org/10.1016/j.applthermaleng.2023.120959.

[3] Y. Zeng, D. Chalise, S. Lubner, et al., A review of thermal physics and management inside lithium-ion batteries for high energy density and fast charging, Energy Storage Mater. 41 (2021) 264–288, https://doi.org/10.1016/j.ensm.2021.06.008.

[4] L. Sheng, Z. Zhang, L. Su, et al., Quasi steady state method to measure thermophysical parameters of cylindrical lithium-ion batteries, J. Power Sources 485 (2021) 229342, https://doi.org/10.1016/j.jpowsour.2020.229342.

[5] J. Liu, S. Yadav, M. Salman, et al., Review of thermal coupled battery models and parameter identification for lithium-ion battery heat generation in EV battery thermal management system, Int. J. Heat Mass Tran. 218 (2024) 124748, https://doi.org/10.1016/j.ijheatmasstransfer.2023.124748.

[6] J. Shi, H. Zhang, H. Yu, et al., Experimental determinations of thermophysical parameters for lithium-ion batteries: a systematic review, eTransportation 20 (2024) 100321, https://doi.org/10.1016/j.etran.2024.100321.

[7] J. Turner, Experimental Measurements of Thermal Characteristics of LiFePO4 Battery, SAE, 2016, pp. 67–77, https://doi.org/10.4271/2015-01-1189.SAETechnicalPaper2015-01-1189.

[8] Y. Yang, X. Huang, Z. Cao, et al., Thermally conductive separator with hierarchical nano/microstructures for improving thermal management of batteries, Nano Energy 22 (2016) 301–309, https://doi.org/10.1016/j.nanoen.2016.01.026.

[9] R. Ponnappan, T. Ravigururajan, Contact thermal resistance of li-ion cell, electrode stack, J. Power Sources 129 (2004) 7–13, https://doi.org/10.1016/j.jpowsour.2003.11.006.

[10] A. Loges, S. Herberger, P. Seegert, et al., A study on specific heat capacities of Li-ion cell components and their influence on thermal management, J. Power Sources 336 (2016) 341–350, https://doi.org/10.1016/j.jpowsour.2016.10.049.

[11] S. Drake, D. Wetz, J. Ostanek, et al., Measurement of anisotropic thermophysical properties of cylindrical Li-ion cells, J. Power Sources 252 (2014) 298–304, https://doi.org/10.1016/j.jpowsour.2013.11.107.

[12] L. Sheng, L. Su, H. Zhang, Experimental determination on thermal parameters of prismatic lithium-ion battery cells, Int. J. Heat Mass Tran. 139 (2019) 231–239, https://doi.org/10.1016/j.ijheatmasstransfer.2019.04.143.

[13] Q. Wu, R. Huang, X. Yu, Measurement of thermophysical parameters and thermal modeling of 21,700 cylindrical battery, J. Energy Storage 65 (2023) 107338, https://doi.org/10.1016/j.est.2023.107338.

[14] C. Wu, M. Tang, W. Peng, et al., Study on the impact of temperature-dependent anisotropic thermal conductivity on thermal diffusion in lithium-ion batteries, J. Power Sources 622 (2024) 235333, https://doi.org/10.1016/j.jpowsour.2024.235333.

[15] X. Feng, S. Wong, T. Chen, et al., An automatic identification method of thermal physical parameter for lithium-ion batteries suffering from thermal runaway, J. Energy Storage 83 (2024) 110358, https://doi.org/10.1016/j.est.2023.110358.

[16] A. Muhammad, S. Shaik, A. Jain, Measurement of radial thermal conductivity of a cylinder using a time-varying heat flux method, J. Therm. Sci. 129 (2018) 301–308, https://doi.org/10.1016/j.ijthermalsci.2018.03.008.

[17] R. Wang, L. Zhao, Z. Yang, Comparison of thermal characteristics of power batteries for electric vehicles, Chinese J. Automot. Eng. 10 (2020) 66–71, https://doi.org/10.3969/j.issn.2095-1469.2020.01.09.

[18] J. Huang, P. Xu, P. Wang, Experimental measurement of anisotropic thermal conductivity of 18650 lithium battery, J. Phys. Conf. 1509 (2020) 012013, https://doi.org/10.1088/1742-6596/1509/1/012013.

[19] Y. Jiang, J. Huang, P. Xu, et al., Axial and radial thermal conductivity measurement of 18,650 Lithium-ion battery, J. Energy Storage 72 (Part C) (2023) 108516, https://doi.org/10.1016/j.est.2023.108516.

[20] L. Sheng, C. Zhang, L. Wang, et al., Experimental-numerical studies on thermal conductivity anisotropy of lithium-ion batteries, J. Energy Storage 103 (Part A) (2024) 114139, https://doi.org/10.1016/j.est.2024.114139.

[21] S. Bo, H. Zhang, Y. Qi, et al., Calculation model of effective thermal conductivity of a spiral-wound lithium-ion battery, J. Therm. Sci. 27 (2018) 572–579, https://doi.org/10.1007/s11630-018-1060-x.

[22] L. Wang, X. Feng, G. Xue, et al., ARC experimental and data analysis for safety evaluation of Li-ion batteries, Energy Storage Sci. Technol. 7 (2018) 1261–1270, https://doi.org/10.12028/j.issn.2095-4239.2018.0161.

[23] N. Nieto, L. Díaz, J. Gastelurrutia, et al., Thermal modeling of large format lithium-ion cells, J. Electrochem. Soc. 160 (2013) A212, https://doi.org/10.1149/2.042302jes.

[24] S. Bazinski, X. Wang, Experimental study on the influence of temperature and state-of-charge on the thermophysical properties of an LFP pouch cell, J. Power Sources 293 (2015) 283–291, https://doi.org/10.1016/j.jpowsour.2015.05.084.

[25] G. Yu, X. Zhang, C. Wang, et al., Experimental study on specific heat capacity of lithium thionyl chloride batteries by a precise measurement method, J. Electrochem. Soc. 160 (2013) A985, https://doi.org/10.1149/2.148306jes.

[26] H. Zhang, L. Sheng, L. Su, Test Method and Device for Specific Heat of Power Battery, CN 108732204A, 2018-05-02.

[27] L. Sheng, L. Su, H. Zhang, et al., An improved calorimetric method for characterizations of the specific heat and the heat generation rate in a prismatic lithium-ion battery cell, Energy Convers. Manag. 180 (2019) 724–732, https://doi.org/10.1016/j.enconman.2018.11.030.

[28] Q. Wu, H. Zhang, J. Li, Calibrated calorimetry for measuring the specific heat and heat generation rate of lithium-ion battery, Automot. Eng. 42 (2020) 59–65, https://doi.org/10.19562/j.chinasae.qcgc.2020.01.009.

[29] M. Faber, O. Buitkamp, S. Ritz, et al., A method to determine the specific heat capacity of lithium-ion battery cells using thermal insulation, J. Power Sources 583 (2023) 233499, https://doi.org/10.1016/j.jpowsour.2023.233499.

[30] Y. Xu, H. Zhang, R. Liu, et al., Analysis of electro-chemical impedance and state of health based on permanent expansion for prismatic batteries, J. Power Sources 605 (2024) 234515, https://doi.org/10.1016/j.jpowsour.2024.234515.

[31] J. Pu, Y. Li, R. Li, Design and performance of a compact lightweight hybrid thermal management system using phase change material and liquid cooling with a honeycomb-like structure for prismatic lithium-ion batteries, J. Power Sources 624 (2024) 235632, https://doi.org/10.1016/j.jpowsour.2024.235632.

[32] H. Zhang, X. Wu, Q. Wu, et al., Experimental investigation of thermal performance of large-sized battery module using hybrid PCM and bottom liquid cooling configuration, Appl. Therm. Eng. 159 (2019) 113968, https://doi.org/10.1016/j.applthermaleng.2019.113968.

[33] J. Zhu, H. Zhang, G. Wu, et al., Thermal performance of cylindrical battery module with both axial and radial thermal paths: numerical simulation and thermal resistance network analysis, J. Energy Storage 49 (2022) 104197, https://doi.org/10.1016/j.est.2022.104197.

[34] W.A. Hermann, Liquid cooling manifold with multi-function thermal interface, U.S. Patent 2010/0104938 A1 Apr. 29 (2010).

[35] C. Zhao, W. Cao, T. Dong, et al., Thermal behavior study of discharging/charging cylindrical lithium-ion battery module cooled by channeled liquid flow, Int. J. Heat Mass Tran. 120 (2018) 751–762, https://doi.org/10.1016/j.ijheatmasstransfer.2017.12.083.

[36] H. Maleki, H. Wang, W. Porter, et al., Li-ion polymer cells thermal property changes as a function of cycle-life, J. Power Sources 263 (2014) 223–230, https://doi.org/10.1016/j.jpowsour.2014.04.033.

[37] F. Incropera, D. DeWitt, T. Bergeman, in: Fundamentals of Heat and Mass Transfer, sixth ed., John Wiley & Sons, Inc, 2007.